circMRPS35 promotes malignant progression and cisplatin resistance in hepatocellular carcinoma

Peng Li,[1,8] Runjie Song,[1,8] Fan Yin,[2] Mei Liu,[3] Huijiao Liu,[1] Shuoqian Ma,[1] Xiaomeng Jia,[1] Xiaohui Lu,[1] Yuting Zhong,[4] Lei Yu,[5] Xiru Li,[4] and Xiangdong Li[1,6,7]

[1]State Key Laboratory of Agrobiotechnology, College of Biological Sciences, China Agricultural University, Beijing 100193, China; [2]Department of Oncology, The Second Medical Centre & National Clinical Research Center of Geriatric Disease, Chinese PLA General Hospital, Beijing 100071, China; [3]Department of Pathology, Chinese PLA General Hospital, Beijing 100071, China; [4]Department of Surgery, Chinese PLA General Hospital, Beijing, 100071, China; [5]Department of Thoracic Surgery, Beijing Tongren Hospital, Capital Medical University, Beijing, 100005, China; [6]Department of Reproduction and Gynecological Endocrinology, Medical University of Bialystok, Bialystok, Poland; [7]Department of Nutrition and Health, China Agricultural University, Beijing 100193, China

Hepatocellular carcinoma (HCC) is one of the major causes of cancer-related death worldwide. Circular RNAs (circRNAs), a novel class of non-coding RNA, have been reported to be involved in the etiology of various malignancies. However, the underlying cellular mechanisms of circRNAs implicated in the pathogenesis of HCC remain unknown. In this study, we identified a functional RNA, hsa_circ_0000384 (circMRPS35), from public tumor databases using a set of computational analyses, and we further identified that circMRPS35 was highly expressed in 35 pairs of HCC from patients. Moreover, knockdown of the expression of circMRPS35 in Huh-7 and HCC-LM3 cells suppressed their proliferation, migration, invasion, clone formation, and cell cycle *in vitro*, and it suppressed tumor growth *in vivo* as well. Mechanically, circMRPS35 sponged microRNA-148a-3p (miR-148a), regulating the expression of *Syntaxin 3* (*STX3*), which modulated the ubiquitination and degradation of phosphatase and tensin homolog (PTEN). Unexpectedly, we detected a peptide encoded by circMRPS35 (circMRPS35-168aa), which was significantly induced by chemotherapeutic drugs and promoted cisplatin resistance in HCC. These results demonstrated that circMRPS35 might be a novel mediator in HCC progress, and they raise the potential of a new biomarker for HCC diagnosis and prognosis, as well as a novel therapeutic target for HCC patients.

INTRODUCTION

Hepatocellular carcinoma (HCC) is one of the most frequently diagnosed cancers and cancer-related deaths globally.[1,2] Due to the lack of symptoms in the early stage of HCC, most patients are usually diagnosed at an advanced stage, and the 5-year survival rate is approximately 14% for HCC patients.[3,4] Therefore, valuable diagnostic biomarkers and therapeutic targets are urgently needed to be explored and verified. In general, surgical resection combined with chemotherapy is curative for the early stage of HCC.[5] However, chemoresistance has been detected in most HCC patients with long-term chemotherapy, leading to a poor prognosis.[6,7] Therefore, the underlying molecular mechanism of chemoresistance in HCC needs further study.

Circular RNAs (circRNAs) are a novel type of non-coding RNA that are covalently closed single-stranded RNAs derived from the back-spliced mechanism of precursor (pre-)mRNA during the process of transcriptions.[8,9] Recently, with the advance of sequencing technologies and bioinformatics approaches, more and more circRNAs have been found, and some of them have been shown to have significant bio-functions.[10] A growing body of evidence shows that circRNAs play important biological roles in the process of HCC tumorigenesis.[11–13]

In this study, by re-analyzing the RNA sequencing (RNA-seq) database from GEO datasets (GEO: GSE77509, GSE114564, and GSE159220), and combined with a series of experimental verifications, we found that hsa_circ_0000384 (circMRPS35) was significantly elevated in HCC. We hypothesized that circMRPS35 might play a crucial role in HCC progression. In order to test our hypothesis, we used the stabilized circMRPS35-knockdown (KD) Huh-7 and HCC-LM3 cell lines to address its critical roles in HCC tumorigenesis both *in vitro* and *in vivo*. Unexpectedly, we found that circMRPS35 encodes a novel peptide with 168 aa upon chemotherapeutic drug treatments, which promoted cisplatin resistance in HCC cells.

Our findings may provide a better understanding of circMRPS35 and its potential novel diagnostic and therapeutic effects on HCC.
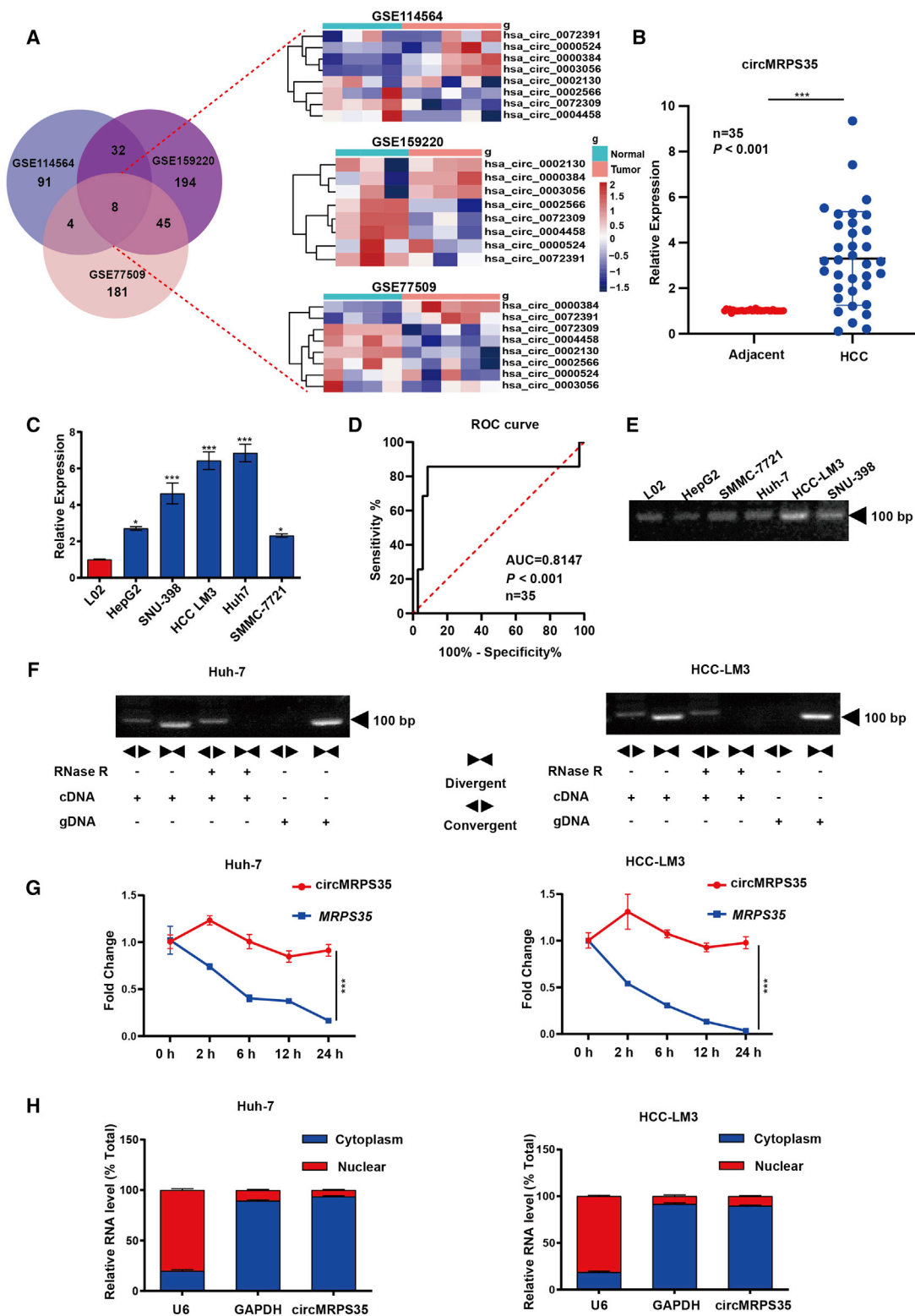
Correspondence: Xiangdong Li, State Key Laboratory of Agrobiotechnology, College of Biological Sciences, China Agricultural University, Beijing 100193, China.
E-mail: xiangdongli68@126.com

Table 1. Association between circMRPS35 expression and clinical features of HCC

Clinical features	N	High expression	Low expression	p Value
Sex				
Male	29	25	4	
Female	6	5	1	0.8973
Age (years)				
<50	16	14	2	
>50	19	16	3	0.8831
Tumor size (cm)				
<5	17	14	3	
>5	18	16	2	0.2858
Lymph node metastasis				
No	25	21	4	
Yes	10	9	1	0.013
HBV infection				
Yes	31	27	4	
No	4	3	1	0.0429
TNM stage				
I–II	14	13	1	
III–IV	21	17	4	0.0564

TNM, tumor-lymph node-metastasis.

RESULTS

The expression and characteristics of circMRPS35 in HCC tissues and cell lines

We mined the RNA-seq database from three GEO datasets (GEO: GSE77509, GSE114564, and GSE159220), and top eight significantly differentially expressed circRNAs in all the three datasets were selected for the further study (Figures 1A and S1A; Tables S2, S3, and S4). Due to four of these eight circRNAs having been thoroughly investigated in HCC studies,[14–17] we then focused on the other four circRNAs. By comparison studies, we found that circMRPS35 was most significantly differentially and highly expressed both in HCC tissues and HCC cell lines (Figures 1B, 1C, and S1B). The receiver operating characteristic (ROC) analysis showed that circMRPS35 yields an excellent diagnostic ability to differentiate between patients with HCC and the unaffected controls (Figure 1D). Based on the clinicopathological characteristics, we further categorized 35 samples of HCC patients into circMRPS35 high- and low-expression groups. We found

that the expression of circMRPS35 was positively correlated with lymph node metastasis and hepatitis B virus (HBV) infection (Table 1). We observed that circMRPS35 was derived from mitochondrial ribosomal protein S35 (MRPS35) with exon 2 to exon 5 (410 bp) of head-to-tail back spliced (Figure S1C). By using a pair of divergent primers crossing its splicing site, we confirmed that circMRPS35 existed and resisted RNase-R digestion in HCC cells (Figures 1E, 1F, and S1D). Moreover, circMRPS35 had a longer half-life than its linear transcript of MRPS35 in Huh-7 and HCC-LM3 cells upon actinomycin D (ACTD) treatment (Figure 1G). The nucleus-cytoplasmic separation analysis showed that circMRPS35 was predominantly localized in the cytoplasm of HCC cells (Figures 1H and S1E). Taken together, these results suggested that circMRPS35 was highly expressed in HCC and was predominantly located in the cytoplasm of HCC cells.

### circMRPS35 acts as an oncogene in HCC cells

To further study the molecular actions of circMRPS35 in HCC cells, we silenced the expression of circMRPS35 by short hairpin RNAs (shRNAs) against the back-spliced sites of circMRPS35 in Huh-7 and HCC-LM3 cells; meanwhile, these shRNAs did not affect the linear transcription of MRPS35 (Figures 2A and 2B). Next, cell viability and colony formation assays demonstrated that the proliferation of Huh-7 and HCC-LM3 cells was suppressed significantly when circMRPS35 was stabilized by KD (Figures 2C and 2D). Subsequently, the wound-healing and transwell assays showed that migration and invasion of the stabilized circMRPS35 KD cells were significantly inhibited (Figures 2E and 2F). The results of flow cytometry showed that cell cycle progression was arrested at the G_0/G_1 phase in the stabilized circMRPS35 KD cells (Figures 2G and 2H). To evaluate the biological functions of circMRPS35 in vivo, shRNA (sh)-circMRPS35-1 or sh-scramble Huh-7 and HCC-LM3 cells were subcutaneously injected into BALB/c nude mice, respectively (n = 6). The growth rate and size (volume and weight) of the xenograft tumors decreased in circMRPS35-stabilized KD tumors (Figures 2I, S2A, and S2B). Moreover, immunohistochemistry (IHC) analysis showed that the expression of Ki67 was significantly decreased in the stabilized circMRPS35 KD tumors (Figure 2J). Taken together, the results showed that suppression of circMRPS35 expression inhibited the proliferation, migration, invasion, cell cycle of HCC cells, and tumor growth both in vitro and in the xenograft tumor models in vivo.

circMRPS35 serves as a sponge for miR-148a in HCC cells

circRNAs can serve as a microRNA (miRNA) sponge through complementary binding sites.[18] We then explored whether circMRPS35

Figure 1. Expression and characteristics of circMRPS35 in HCC tissues and cells

(A) Schematic illustration showing the significantly different expressions of circRNAs predicted by overlapping GEO: GSE77509, GSE114564, and GSE159220 data (left) and an expression heatmap of those overlapping circRNAs (right). (B) Quantitative real-time PCR analysis of circMRPS35 in 35 pairs of HCC and adjacent tissues. (C) Quantitative real-time PCR analysis of circMRPS35 in HCC cell lines compared to L02 cells. (D) ROC curve of the diagnostic value of circMRPS35. (E) RT-PCR analysis of circMRPS35 in HCC cell lines and L02 cells. (F) RT-PCR analysis of circMRPS35 and MRPS35 with divergent and convergent primers after RNase R treatment. (G) Quantitative real-time PCR analysis of circMRPS35 and MRPS35 after ACTD treatment. (H) Quantitative real-time PCR analysis of circMRPS35 after RNA nucleocytoplasmic separation, with U6 and GAPDH as markers of the nucleus and cytoplasm in Huh-7 and HCC-LM3 cells, respectively. Error bars represent the means ± SEM of three independent experiments. *p < 0.05, **p < 0.01, ***p < 0.001.
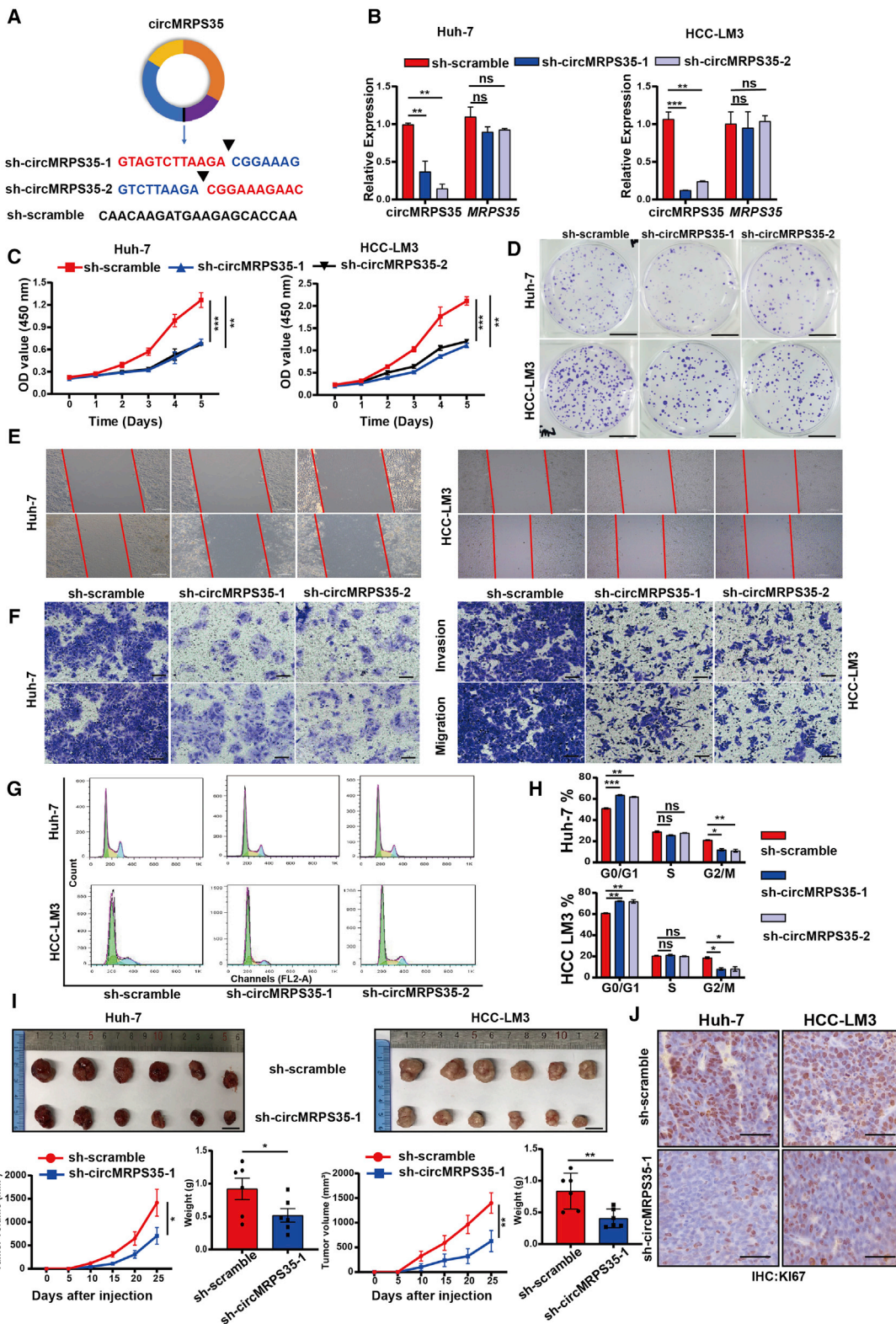
promoted HCC progress by interacting with miRNAs. A list of 24 potential miRNAs that might directly bind to circMRPS35 were generated through screening bioinformatics databases (miRanda, ENCORI, and circBank) (Figure 3A; Table S5). In addition, we screened out four miRNAs (miR-148a, miR-23c, miR-676, miR-421) of this list with significantly different expressions and poor prognosis in HCC for the further study by reanalyzing The Cancer Genome Atlas (TCGA) RNA-seq data (Figures 3B, S3A, and S3B). Anti-argonaute 2 (AGO2) complex RNA immunoprecipitation (RIP) assays were routinely used to purify the interactive miRNAs.[19] We confirmed that AGO2 could accumulate circMRPS35 and the above four miRNA candidates; however, only miR-148a was significantly accumulated by circMRPS35, which suggested that miR-148a was associated with circMRPS35 in HCC cells (Figures 3C, 3D, and S3C).

miR-148a belongs to the miR-148a/148b/152 family with highly identical sequences (Figure S3E). We found that the expressions of miR-148a/148b/152 were significantly decreased in HCC tissues and HCC cell lines (Figures 3E and 3F). Moreover, the expression of circMRPS35 was negatively correlated with the expression of miR-148a/148b/152 (Figure 3G). Unexpectedly, we found that miR-148a had significantly higher expression and presented a worse prognosis than those of miR-148b and miR-152 in HCC via re-analyzing TCGA RNA-seq data (Figures S3F and S3G). Thus, we estimated that miR-148a might play the most important role in HCC progression compared with miR-148b and miR-152. Notably, by analyzing circMRPS35 in the TargetScan database, we found that circMRPS35 had four binding sites with miR-148a (Figure S3H). The dual-luciferase reporter results showed that the miR-148a mimic decreased the relative luciferase intensity of the circMRPS35 containing luciferase vector, compared with the four sites of mutant (Mut) vector in Huh-7 and HCC-LM3 cells. (Figures 3H and S3I). In addition, a series of rescue assays showed that the suppressed effects of miR-148a in HCC cells were reversed by the stabilized circMRPS35 overexpression in both Huh-7 and HCC-LM3 cells (Figures 3I–3K). Overall, these results provided the evidence that the oncogenic functions of circMRPS35 were acted on via sponging miR-148a in HCC.

circMRPS35 sponges miR-148a to regulate the expression of STX3 in HCC cells

By using multiple databases (TargetScan, miRWalk, miRDB, and TCGA), we screened out five downstream targets of the circMRPS35-miR-148a axis, including syntaxin 3 (STX3), leptin receptor overlapping transcript like 1 (LEPROTL1), macrophage immunometabolism regulator (MACIR), tyrosine 3-monooxygenase/tryptophan 5-monooxygenase activation protein β (YWHAB), and ubiquitin conjugating enzyme E2 D1 (UBE2D1), which were significantly highly expressed in HCC and negatively correlated with the expression of miR-148a (Figures 4A–4C and S4A–S4D). Further studies showed that these five genes were highly expressed in HCC cells (Figures 4D and S4E–S4H). However, only STX3 was markedly decreased by overexpression of miR-148a in Huh-7 and HCC-LM3 cells, and this higher STX3 expression further presented the worse prognosis in HCC patients (Figure 4E, 4F, and S4I–S4L). In addition, we confirmed that STX3 was highly expressed in HCC tissues (Figures 4G and 4H). In parallel, the expression of circMRPS35 was positively correlated with the expression of STX3 in HCC tissues (Figure 4I). Moreover, we found that miR-148a mimic decreased the relative luciferase intensity of the STX3 3′ untranslated region (UTR)-contained luciferase vector, compared with the Mut vector in Huh-7 and HCC-LM3 cells (Figure 4J). Furthermore, the expression of STX3 was significantly decreased in the stabilized circMRPS35 KD or miR-148a overexpressed Huh-7 and HCC-LM3 cells (Figures 4K and 4L), respectively. Overall, we demonstrated that circMRPS35 could sponge miR-148a, which in turn regulates the expression of STX3.

The stability of PTEN is regulated by circMRPS35 and STX3 in HCC cells

A previous study showed that STX3 could degrade phosphatase and tensin homolog (PTEN) by increasing its ubiquitination in breast cancer.[20] We then tested whether circMRPS35 could promote the degradation of PTEN through regulating the expression of STX3 in HCC. Two specific small interfering RNAs (siRNAs) were designed to silenced the expression of STX3 in Huh-7 and HCC-LM3 cells. We observed that silenced STX3 did not change the mRNA level of PTEN compared with control cells (Figures 5A, S5A, and S5B). However, the protein level of PTEN was upregulated in STX3-silenced cells, which indicated that STX3 might regulate the stability of PTEN (Figure 5B). By using both the anti-STX3 and anti-PTEN antibodies, we showed that PTEN could interact with STX3 in Huh-7 and HCC-LM3 cells in IP assays (Figure 5C). Then, we found that overexpressing of STX3 increased the ubiquitin signals of PTEN in 293T cells, and the ubiquitin signals of PTEN were also decreased in STX3-silenced Huh-7 and HCC cells (Figures 5D and 5E).

Figure 2. circMRPS35 acts as an oncogene in HCC cells

(A) Schematic representation of target sequences of shRNAs of circMRPS35. (B) Quantitative real-time PCR analysis of circMRPS35 and MRPS35 of circMRPS35 KD Huh-7 and HCC-LM3 cells. (C) Cell viability assays were used to test proliferation of circMRPS35 KD or control Huh-7 and HCC-LM3 cells. (D) Colony formation assays were performed to test cell growth of circMRPS35 KD or control Huh-7 and HCC-LM3 cells (scale bars, 1 cm). (E) Wound-healing experiments were used to detect cell migration of circMRPS35 KD or control Huh-7 and HCC-LM3 cells (scale bars, 100 μm). (F) Transwell assays of invasion and migration in circMRPS35 KD or control Huh-7 and HCC-LM3 cells (scale bars, 100 μm). (G and H) Cell cycle assays were used to detect cell cycle arrest levels of circMRPS35 KD or control Huh-7 and HCC-LM3 cells: G_0/G_1, green only; S, yellow; G_2/M, blue only. (I) BALB/c nude mice (n = 6 each group) were injected sh-circMRPS35-1 or sh-scramble Huh-7 and HCC-LM3 cells. Sizes of xenograft tumors were measured every 5 days, and weights of xenograft tumors were summarized after animals were sacrificed (scale bars, 1 cm). (J) IHC analysis of Ki67 for sh-circMRPS35-1 or sh-scramble Huh-7 and HCC-LM3 xenograft tumors tissues (scale bars, 100 μm). Error bars represent the means ± SEM of three independent experiments. *p < 0.05, **p < 0.01, ***p < 0.001.
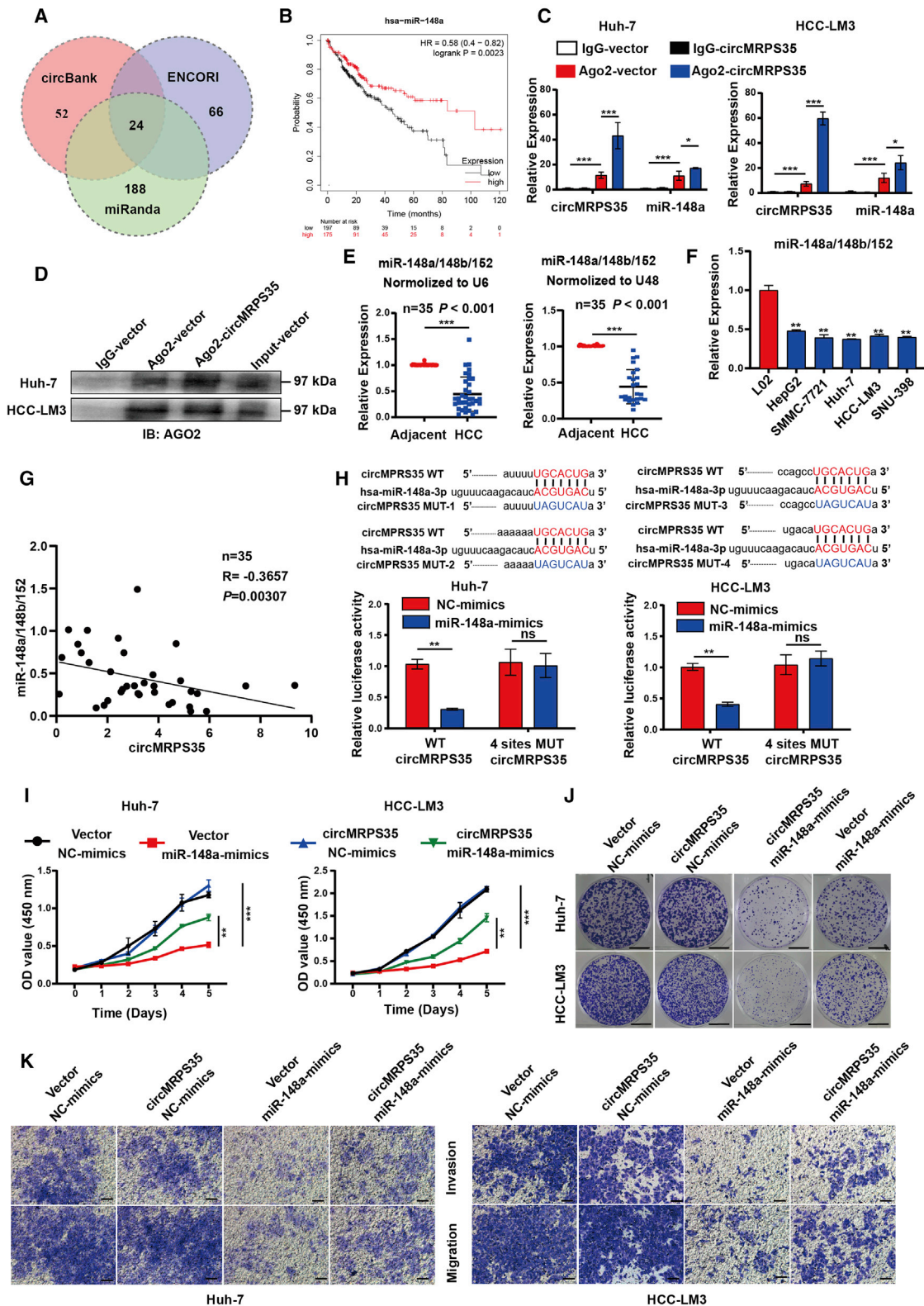
(legend on next page)

Furthermore, we also showed that the protein level of PTEN was upregulated in stabilized circMRPS35 KD cells without alteration in the mRNA level of *PTEN* (Figures 4L, S5C, and S5D), and the ubiquitin signals of PTEN were decreased in stabilized circMRPS35 KD Huh-7 and HCC-LM3 cells (Figure 5F). In addition, we showed that circMRPS35 KD Huh-7 and HCC-LM3 cells increased the stability of PTEN (Figures 5G and 5H). Overall, we demonstrated that circMRPS35 could regulate PTEN stability through the circMRPS35-miR-148a-STX3 axis in HCC cells.

Chemotherapy induces the translation of circMRPS35-168aa in HCC

By further re-analyzing the RNA-seq database (GEO: GSE140202), we found that circMRPS35 was highly expressed in the sorafenib-treated group in HCC (Figure 6A), which indicated that circMRPS35 might be related to chemotherapy. We then used five commonly used chemotherapeutic drugs (doxorubicin [DOX], ACTD, etoposide, cisplatin, and sorafenib) to treat Huh-7 and HCC-LM3 cells and found that circMRPS35 was most highly elevated with cisplatin treatment (Figure 6B). However, the expressions of STX3 and miR-148a were not changed in cisplatin-treated cells, which revealed that the circMRPS35 might have other functions in HCC cells rather than sponging miR148a in cisplatin treatment (Figures S6A–S6C). By analysis from using circRNADb, we found that circMRPS35 has two internal ribosome entry site (IRES) putative regions (IRES 1, 14–158 sites; IRES 2, 81–161 sites) that potentially code a 168-aa peptide (Figure S6D). We confirmed that IRES 1 induced high firefly luciferase (F-Luc)/Renilla luciferase (R-Luc) activity compared with the negative control and IRES 2 (Figure 6C). The translation process of circRNAs could be associated with polyribosome (polysome).[21,22] The results of separation of polysome fractionation showed that circMRPS35 was present in all polysome fractions in HCC-LM3 and Huh-7 cells (Figure 6D). Then we used IP of FLAG antibody in circMRPS35-FLAG-overexpressed Huh-7 cells, and the 20-kDa band was further detected and identified as circMRPS-168aa by liquid chromatography-mass spectrometry (LC-MS) (Figures 6E and 6F). Due to 115 aa of circMRPS35-168aa that originated from MRPS35, we used an MRPS35 antibody to test this peptide and found that circMRPS35-168aa was significantly induced by cisplatin, DOX, and etoposide (Figure 6G). Taken together, we demonstrated that circMRPS35 contemporarily encoded an uncharacterized peptide induced by multiple chemotherapeutic drugs in HCC cells.

circMRPS35-168aa resists the cisplatin treatment in HCC cells

We used cisplatin, DOX, etoposide, and ACTD to identify whether the sensitivity of these drugs was regulated by circMRPS35. The results showed that stabilized circMRPS35 KD mostly inhibited the cell viability of cells treated with cisplatin, while the overexpressed circMRPS35-168aa mostly induced cisplatin resistance (Figures 7A and S7A–S7D). The half-maximal inhibitory concentration (IC_{50}) was also decreased in stabilized circMRPS35 KD cells and increased in circMRPS35-168aa overexpressed cells with cisplatin treatment (Figure 7B). Apoptosis analysis showed that the apoptosis rate decreased in circMRPS35-168aa overexpressed Huh-7 and HCC-LM3 cells with cisplatin treatment (Figures 7C and 7D). Western blot results showed that the high expression of circMRPS35-168aa counteracted the cisplatin-induced high level of cleaved caspase-3 (c-caspase-3) (Figure 7E). In summary, our results showed that circMRPS35-168aa can play a critical role in cisplatin resistance in HCC cells.

DISCUSSION

circRNAs, characterized by high stability and conservation, have been increasingly demonstrated to function as novel promising therapeutic RNA molecules for diverse human diseases, including cancers.[23] In this study, we determined that circMRPS35 was significantly upregulated in HCC and that stabilized silenced expression of circMRPS35 suppressed the growth, migration, invasion, and cell cycle progression of HCC cells. Furthermore, we demonstrated that circMRPS35 encoded a novel peptide (circMRPS35-168aa), which was significantly induced by chemotherapeutic drugs and promoted cisplatin resistance in HCC cells. We demonstrated that circMRPS35 might be a novel mediator in HCC progress, which raises its potential as a new biomarker for HCC diagnosis and prognosis, as well as a novel therapeutic target for HCC patients.

Mechanistically, multiple functions of circRNAs were shown in HCC.[24,25] For example, circMTO1 acted as an endogenous sponge for miR-9 to regulate the progression of HCC;[11] circZKSCAN1 served as the sponge for fragile X mental retardation protein (FMRP) to suppress the Wnt/β-catenin signaling pathway in HCC;[12] and circβ-catenin coded a peptide to promote the progression of HCC.[13] However, in this study, we found that circMRPS35, on the one hand, acted as a miRNA sponge, forming a circMRPS35-miR148a-STX3-PTEN axis to control malignant progression of HCC cells. On the other hand, circMRPS35 encoded a novel 168-aa peptide endowing the HCC cells with chemoresistance in cisplatin treatment.

Figure 3. circMRPS35 serves as a sponge for miR-148a in HCC cells

(A) Schematic illustration of the target miRNAs of circMRPS35 predicted by overlapping miRanda, ENCORI, and circBank databases. (B) Kaplan-Meier analysis of miR-148a in HCC (n = 364). (C) Quantitative real-time PCR analysis of circMRPS35 and miR-148a with AGO2-RIP in Huh-7 and HCC-LM3 cells. (D) Western blot analysis of AGO2 protein level in Huh-7 and HCC-LM3 cells. (E) Quantitative real-time PCR analysis of miR-148a/148b/152 in 35 pairs of HCC and adjacent tissues normalized to U6 or U48. (F) Quantitative real-time PCR analysis of miR-148a/148b/152 in HCC cell lines compared to L02 cells. (G) Correlation analysis of circMRPS35 and miR-148a/148b/152 expression (n = 35). (H) Predicted complementary binding sites between circMRPS35 and miR-148a (up) and a luciferase reporter assay were used to test the binding of miR-148a and circMRPS35 in Huh-7 and HCC-LM3 cells (down). (I–K) Co-transfection with miR-148a mimics and circMRPS35 to test the proliferation assays (I), colony formation assays (scale bars, 1 cm) (J), and migration and invasion assays (scale bars, 100 μm) (K) in Huh-7 and HCC-LM3 cells. Error bars represent the means ± SEM of three independent experiments. *p < 0.05, **p < 0.01, ***p < 0.001.
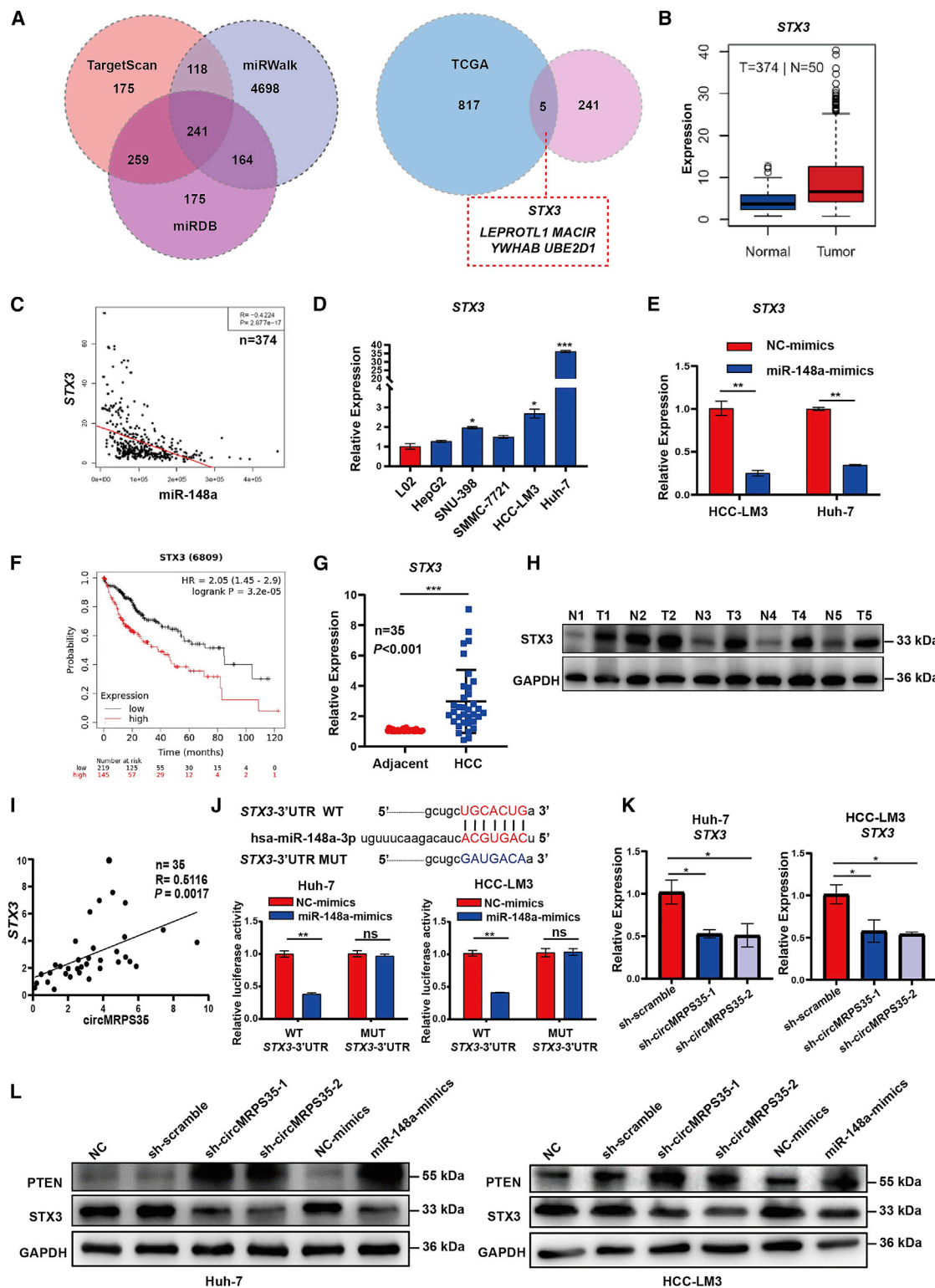
Figure 4. circMRPS35 sponges miR-148a to regulate the expression of STX3 in HCC cells

(A) Schematic illustration showing the target mRNAs of miR-148a predicted by overlapping TargetScan, miRWalk and miRDB databases (left) and the HCC TCGA database (right). (B and C) TCGA analysis of expression of *STX3* in HCC tissues and correlation analysis of miR-148a and *STX3* expression. (D) Quantitative real-time PCR assays of

(legend continued on next page)

Many studies have shown that miR-148a is an important tumor suppressor and a potential biomarker with its low expression in HCC.[26–30] To our knowledge, studies have mainly focused on the functions of miR-148a, but the regulators of miR-148a were rarely reported in HCC. In this study, we showed that circMRPS35 acted as a regulator to sponge miR-148a, which in turn regulated the pre-mRNA degradation of *STX3* through the RNA-induced silencing complex (RISC). STX3 is a member of soluble *N*-ethylmaleimide-sensitive factor attachment protein receptor (SNARE) family localized in plasma membrane, mediating vesicular trafficking and exocytosis.[31–33] However, the potential roles of STX3 in HCC remain unknown. In this study, we put forward that STX3 promoted the degradation of PTEN through STX3 mediating ubiquitin in HCC.

Notably, increased cisplatin chemoresistance is the main clinical problem of HCC chemotherapy; however, the mechanisms of cisplatin chemoresistance remain unclear.[34–36] A few studies have shown that circRNAs are relatively resistant to cisplatin in HCC. For instance, circRNA_102272 was upregulated by cisplatin treatment and promoted cisplatin resistance via sponging miR-326 to regulate the RUNX2 axis.[37] In this study, we showed that cisplatin promoted the expression of circMRPS35-168aa, which led to cisplatin resistance via suppressing cisplatin-induced apoptosis.

For cell apoptosis, the release of cytochrome *c* from the mitochondria caused by the increase of mitochondrial outer membrane permeabilization activated the cleavage of caspase-3.[38,39] Furthermore, circMRPS35-168aa was predicted as a mitochondrial-localized peptide by Cell-PLoc 2.0. Base on the above findings, future studies may be necessary to elucidate the mechanical possibility of circMRPS35-168aa participating in the regulation of mitochondrial outer membrane permeabilization to inhibit cisplatin-induced apoptosis.

A previous study showed that circMRPS35 was expressed at a low level and acted as a protein sponge of lysine acetyltransferase 7 (KAT7) for histone acetylation to regulate the transcription of *FOXO1* and *FOXO3a* in gastric cancer.[40] In contrast to this gastric cancer study, we found that circMRPS35 was highly expressed and had other multiple functions in HCC. This discrepancy may be due to the complicated roles of circMRPS35 in various cancers, and the actions of circMRPS35 may depend on the context of its binding targets inside the particular cells, or under various conditions.

It is well known that the biogenesis of circRNAs was regulated by the RNA-binding proteins (RBPs).[41] For example, FUS RBP regulated circRNA biogenesis in motor neurons derived from murine embryonic stem cells,[42] and heterogeneous nuclear ribonucleoprotein L (HNRNPL) circularized circARHGAP35 in HCC.[43] In a future study, we will analyze the potential binding of RBPs for *MRPS35*-specific motifs in the flanking introns combined with the HCC different RBP expression profiles to clarify the potential biogenesis regulators of circMRPS35 in HCC.

In our current study, the clinical evidence of circMRPS35 was still limited, and the correlation between circMRPS35 and clinical diagnosis, prognosis, pathogenesis, and chemoresistance of HCC in a large clinical trial needed to be further studied. In future studies, we will continue collecting HCC tissues (with or without chemotherapy) and recording the corresponding follow-up information to investigate the relationship between circMRPS35 and the prognostication of HCC.

In summary, by using functional verification together with clinical evidence, the present study demonstrates that circMRPS35 could be a crucial regulator for the progression and chemoresistance in HCC with its different expression pattern under different conditions. circMRPS35 not only elicited its oncogenic role in HCC through sponging miR-148a to regulate the STX3-PTEN axis, but also by encoding circMRPS35-168aa, leading to cisplatin resistance (Figure 7F).

Taken together, we showed that circMRPS35 has the potential to be a biomarker to predict prognosis for HCC therapy and a therapeutic target for HCC, especially in HCC chemoresistance.

MATERIALS AND METHODS

Patients and tissue samples
In this study, 35 pairs of HCC and their corresponding adjacent tissues were collected and stored at $-80°C$ from patients who underwent surgery at the Chinese PLA General Hospital between 2018 and 2020. None of the patients was treated with either chemotherapy or radiation prior to surgery. Clinical data of patients are summarized in Table 1.

Bioinformatics analysis
For circRNA expression analysis, HCC RNA-seq data (GEO: GSE77509, GSE114564, and GSE159220) were downloaded from the NCBI SRA database. CIRI2, CIRCexplorer2, and find_circ were used for characterization of circRNAs.[44] HISAT2, Bowtie2, and StringTie were performed to re-assemble the sequencing transcriptome after aligning to reference genome human GRCh37. Then, the quantification of these circRNAs was performed by using a modified version of edgeR in CIRIquant, and circBase was used for

---

STX3 expression in HCC cell lines compared to L02 cells. (E) Quantitative real-time PCR assays of *STX3* in miR-148a overexpression HCC-LM3 and Huh-7 cells. (F) Kaplan-Meier analysis of the expression of *STX3* in HCC (n = 364). (G) Quantitative real-time PCR analysis of *STX3* in 35 pairs of HCC and adjacent tissues (n = 35). (H) Western blot analysis of STX3 in five pairs of HCC and adjacent tissues. (I) Correlation analysis of circMRPS35 and *STX3* expression (n = 35). (J) Predicted complementary binding sites between *STX3* and miR-148a (upper); a luciferase reporter assay was used to test the binding of *STX3* and miR-148a in Huh-7 and HCC-LM3 cells (lower). (K) Quantitative real-time PCR assays of *STX3* in circMRPS35 KD or control Huh-7 and HCC-LM3 cells. (L) Western blot analysis of STX3 and PTEN in circMRPS35 KD and miR-148a overexpression and control Huh-7 and HCC-LM3 cells. Error bars represent the means ± SEM of three independent experiments. *p < 0.05, **p < 0.01, ***p < 0.001.
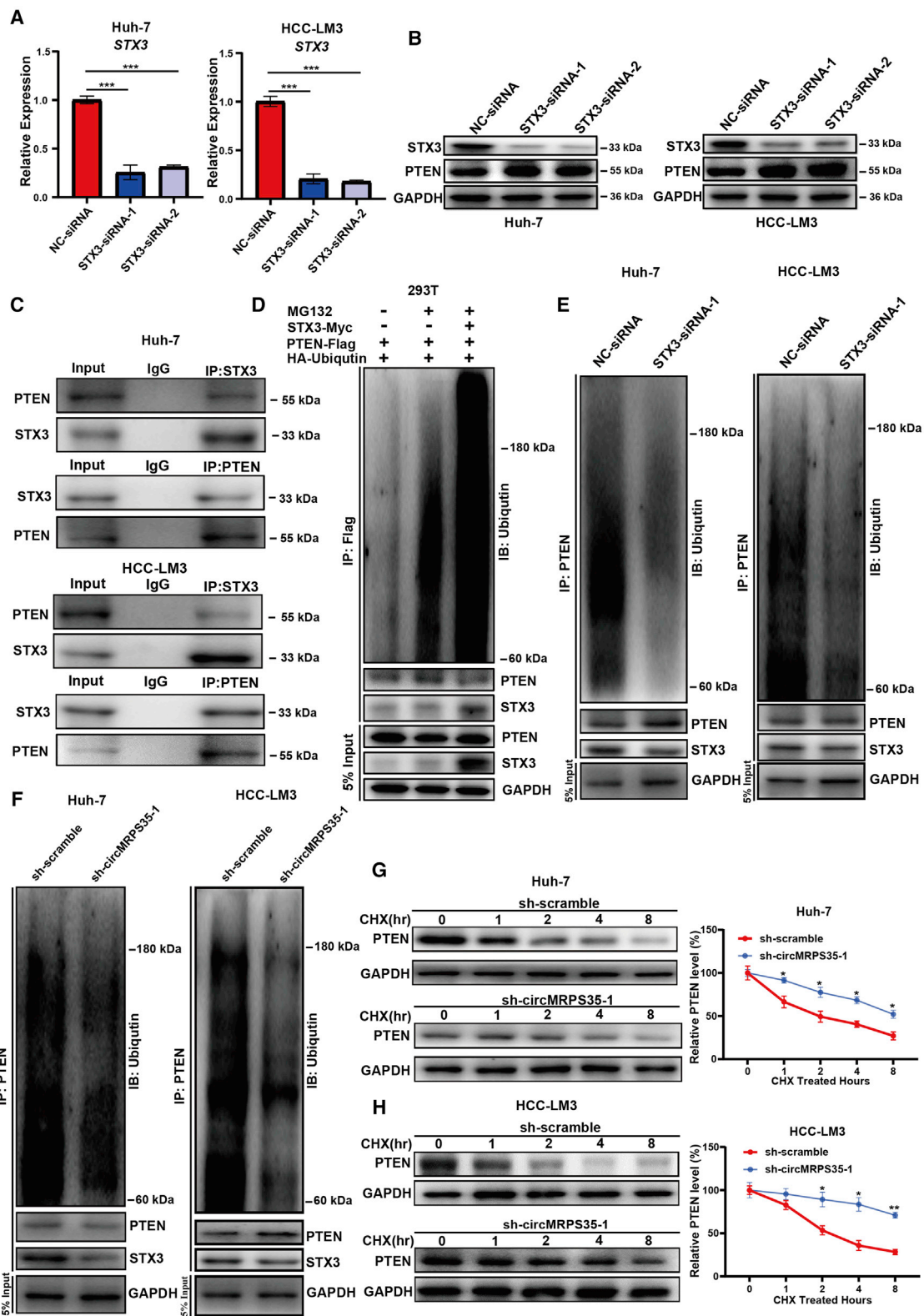
(legend on next page)

annotation of these circRNAs. The differentially expressed circR-NAs were identified by using the edgeR package (version 3.12.1) with general linear model, and a fold change >2 and p value <0.05 were recognized as significantly differentially expressed circRNAs. The expressions of miRNAs and mRNA were generated by the ggboxplot or pheatmap R package via analysis of TCGA HCC RNA-seq data (https://www.cancer.gov/about-nci/organization/ccg/research/structural-genomics/tcga). Kaplan-Meier curves of overall survival in HCC patients were drawn by using the Kaplan-Meier Plotter (http://kmplot.com/analysis/). The localization of circMRPS35 was predicted by Cell-PLoc 2.0 (http://csbio.sjtu.edu.cn/bioinf/Cell-PLoc-2/).

Cell culture

Human 293T cells, human HCC cell lines HepG2, SNU-398, SMMC-7721, Huh-7, and HCC-LM3, and the human normal liver cell line L02 were used in the present study. The cell lines of 293T and HepG2 were purchased from the Cell Bank of the Peking Union Medical College Hospital (Beijing, China). The other cell lines were a generous gift from the State Key Laboratory of Proteomics, Beijing Proteome Research Center, Beijing Institute of Radiation Medicine (Beijing, China). L02 and SNU-398 cell lines were cultured in Roswell Park Memorial Institute 1640 medium (Gibco, Carlsbad, CA, USA), and other cell lines were cultured in Dulbecco's modified Eagle's medium (DMEM, Gibco) with 10% fetal bovine serum (FBS, Gibco) at 37°C with 5% CO_2.

RNA extraction and reverse transcription

Total RNAs were extracted from cell lines and tissues using TRIzol (Invitrogen, Carlsbad, CA, USA) according to the manufacturer's instructions. cDNAs were synthesized from total RNA using Moloney murine leukemia virus (M-MLV) reverse transcriptase (Takara, Dalian, China) based on the manufacturer's instructions.

RNase R treatment and ACTD assay

Total RNAs were treated with RNase R for 30 min at 37°C using 3 U/mg RNase R (Epicenter Technologies, Madison, WI, USA). HCC-LM3 and Huh-7 cells were treated with ACTD (1 μg/mL) (Sigma-Aldrich, St. Louis, MO, USA) at 0, 2, 6, 12, and 24 h before RNA extraction.

Nucleocytoplasmic separation

The RNA of nuclear and cytoplasmic fractions was separated and extracted using a Paris kit (Invitrogen) according to the manufacturer's instructions.

Reverse transcriptase PCR (RT-PCR) and quantitative real-time PCR

RT-PCR was conducted using PrimeSTAR Master Mix (Takara) according to manufacturer's instructions along with PCR control. Products were separated on a 2% agarose gel and visualized with GelRed (Beyotime, Shanghai, China). Quantitative real-time PCR analyses were performed by using SYBR Green PCR master mix (Invitrogen) with the StepOnePlus system (Invitrogen) according to the manufacturer's instructions. *GAPDH* was used as the internal control to normalize circMRPS35; *MRPS35*, *STX3*, *PTEN*, U6, and U48 were used as internal controls to normalize miR-148a/miR-148b/miR-152. The relative expression of target genes was calculated by the $2^{-\Delta\Delta Ct}$ method. Primers are listed in Table S1.

Oligonucleotide synthesis, plasmid construction, and transfection

The oligonucleotides of miR-148a mimics, control mimics, *STX3*-siRNA-1, *STX3*-siRNA-2, and negative control (NC)-siRNA were synthesized by GenePharma (Suzhou, China). Two specific shRNAs for circMRPS35 designed to target the covalent closed junction were cloned into PLKO.1-TRC plasmid to silence the expression of circMRPS35. The PLO5-ciR plasmid (Geneseed, Guangzhou, China) containing the sequence of circMRPS35 was constructed and used to upregulate circMRPS35 expression. The PLV plasmid containing the sequence of circMRPS35-168aa was constructed and used to upregulate circMRPS35-168aa expression. The coding sequences of STX3-Myc and PTEN-FLAG were constructed in PLV plasmid and used to upregulate the expression of STX3-Myc and PTEN-FLAG. For the dual-luciferase reporter gene assay, wild-type (WT) and Mut of miR-148a putative binding sites reporter plasmids were constructed using the circMRPS35 and 3′ UTR of *STX3* sequences in the psiCHECK2 vector (Promega, Madison, WI, USA). For IRES activity analysis, the promoter region of F-Luc in the psiCHECK2 vector was deleted and the IRES sequences of circMRPS35 were cloned behind R-Luc. Plasmids, miR-148a mimics, control mimics, *STX3*-siRNA-1, *STX3*-siRNA-2, and NC-siRNA were transfected, respectively, into cells by using Lipofectamine 3000 (Invitrogen) based on the manufacturer's instructions.

Lentivirus packaging, infection, and puromycin selection

Vectors (PLKO.1-sh-circMRPS35-1, PLKO.1-sh-circMRPS35-2, PLKO.1-sh-scramble, PLV, PLO5-ciR, PLO5-ciR-circMRPS35, PLO5-ciR-circMRPS35-FLAG, and PLV-circMRPS35-168aa) were co-transfected, respectively, with packaging plasmids psPAX2

Figure 5. The stability of PTEN is regulated by circMRPS35 and STX3 in HCC cells

v(A) Quantitative real-time PCR assays of *STX3* in *STX3* silenced or control Huh-7 and HCC-LM3 cells. (B) Western blot analysis of STX3 and PTEN in *STX3* silenced or control Huh-7 and HCC-LM3 cells. (C) IP by anti-IgG, anti-PTEN, or anti-STX3 antibodies and western blot analysis of PTEN and STX3 in Huh-7 and HCC-LM3 cells. (D) 293T cells were transfected and treated with/without MG132, and then cells were immunoprecipitated with anti-FLAG antibodies and western blot by indicated antibodies. (E) *STX3* silenced or control Huh-7 and HCC-LM3 cells were treated with MG132; cells were immunoprecipitated with anti-PTEN antibodies and western blot by indicated antibodies. (F) circMRPS35 KD or control Huh-7 and HCC-LM3 cells were treated with MG132; cells were immunoprecipitated with anti-PTEN antibodies and western blot by indicated antibodies. (G and H) circMRPS35 KD or control Huh-7 and HCC-LM3 cells were treated with CHX for indicated times; western blot and quantification of relative PTEN protein levels are shown. Error bars represent the means ± SEM of three independent experiments. *p < 0.05, **p < 0.01, ***p < 0.001.
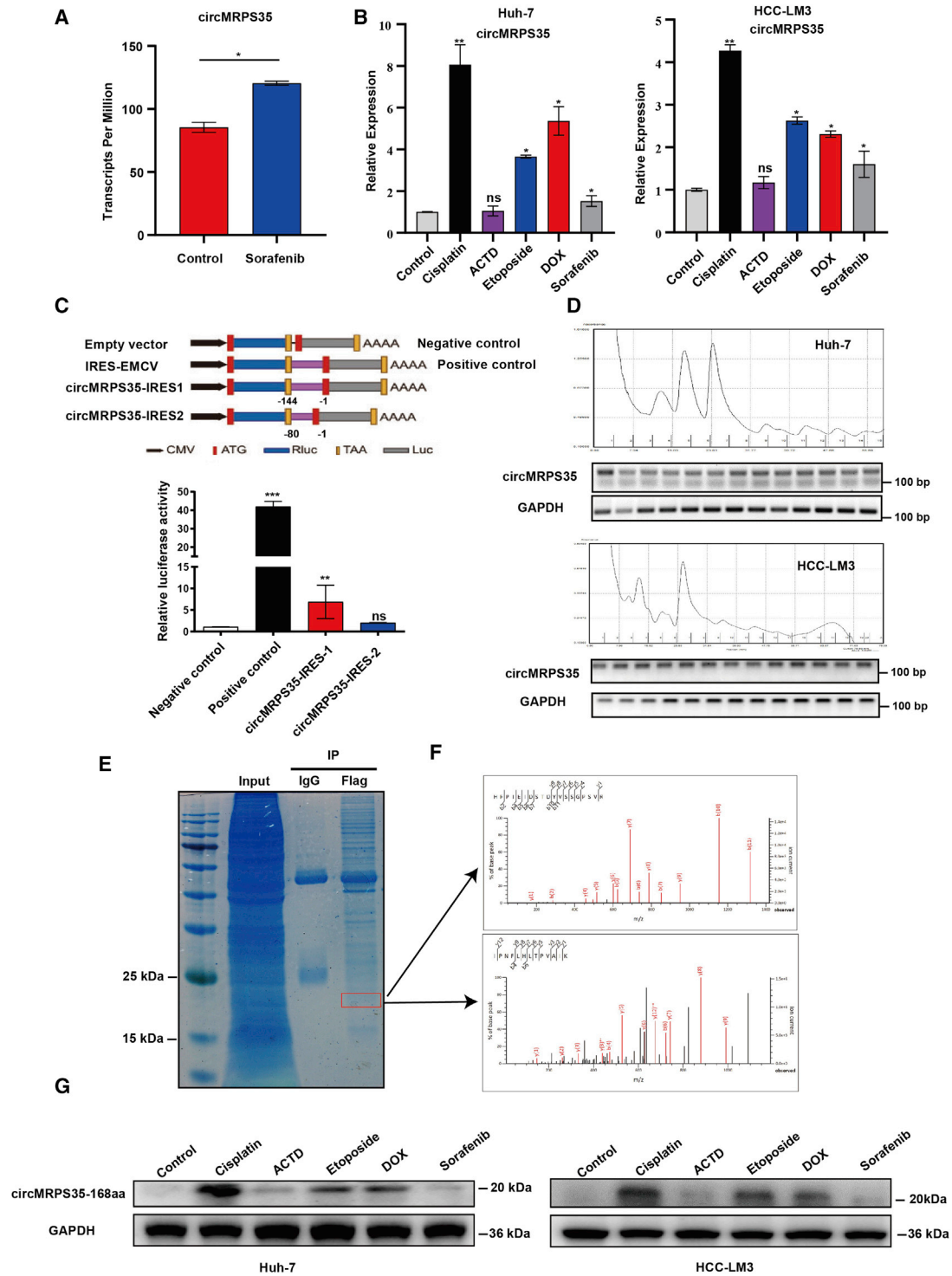
Figure 6. Chemotherapy induces the expression of circMRPS35 and translation of circMRPS35-168aa

(A) RNA-seq (GEO: GSE140202) analyses of circMRPS35 in sorafenib-treated cells compared to non-treated cells. (B) Quantitative real-time PCR analysis of circMRPS35 after DOX, etoposide, ACTD, and cisplatin treatment or non-treated Huh-7 and HCC-LM3 cells. (C) Schematic illustration showing that IRESs in circMRPS35 were cloned between R-Luc and F-Luc reporter genes with independent start and stop codons (upper). The relative luciferase activity of F-Luc/R-Luc in the above vectors was tested in

(legend continued on next page)

and pMD2.G into 293T cells. Infectious supernatant was harvested at 48 and 72 h after transfection and filtered through 0.45-μm filters (Millipore, Billerica, MA, USA). Huh-7 and HCC-LM3 cells were infected with recombinant lentivirus at a multiplicity of infection (MOI) of 15 and 40, respectively, for 48 h and then selected by 3 and 1 μg/mL puromycin (Sigma-Aldrich) for 72 h.

Cell proliferation assays and wound-healing assay

Huh-7 and HCC-LM3 cells were reseeded in 96-well plates (1×10^3 cells per well), and the cell viability was detected by Cell Counting Kit-8 (CCK-8, Beyotime) with absorbance of a wavelength of 450 nm for each well. For cell colony formation assays, the treated Huh-7 and HCC-LM3 cells were placed in six-well plates (3×10^3 cells per well) incubated at 37°C with 5% CO_2 for 7 days. Cells were stained with crystal violet staining solution (Beyotime). For the wound-healing assay, the treated Huh-7 and HCC-LM3 cells from different groups were placed in six-well plates (4×10^4 cells per well) with serum-free medium. Constant-diameter strips were scratched in the confluent monolayers with a 10-μL sterile Eppendorf pipette tip. The width of scratches was obtained at 0 and 48 h in the same places using a microscope (Ti-U, Nikon, Tokyo, Japan).

Migration and invasion assays

Transwells (8-mm pore size, Corning Life Sciences, NY, USA) were used for invasion and migration assays. For migration assays, Huh-7 and HCC-LM3 cells were reseeded in small chambers (2×10^4 cells per well), and 600 μL of cell culture medium was added in the bottom chambers at 37°C with 5% CO_2 for 48 h. For invasion assays, the small chambers were first coated with 100 μL of Matrigel (Invitrogen) for a 30-min incubation at 37°C, and then Huh-7 and HCC-LM3 cells were reseeded in the small chambers (2×10^4 cells per well) and 600 μL of cell culture medium was added in the bottom chambers at 37°C with 5% CO_2 for 48 h. Cells were stained with crystal violet staining solution (Beyotime) and inner cells of small chambers were removed. The outer cells were imaged randomly with a microscope (Nikon).

Cell cycle analysis

Treated Huh-7 and HCC-LM3 cells (2×10^5 cells) were digested by trypsin, washed twice with PBS, and fixed 4 h at 4°C in 70% ethanol. Cells were washed with PBS and strained with a cell cycle analysis kit (Beyotime). Flow cytometry (BD Biosciences, Franklin Lakes, NJ, USA) was used to analyze the staining, and the data were analyzed with FlowJo 7.6 software (Tree Star, San Francisco, CA, USA).

Dual-luciferase reporter gene assay

Huh-7 and HCC-LM3 cells were co-transfected with WT or Mut circMRPS35, STX3 3′ UTR, and miR-148a-mimics or NC-mimics. R-Luc activity was normalized to F-Luc. For IRES activity analysis, 293T cells with transfected with IRES-contained plasmids. F-Luc activity was normalized to R-Luc activity. After transfection for 48 h, cells were subjected to dual-luciferase analysis. Luciferase activity was assessed using the dual-luciferase reporter kit (TransGene, Beijing, China) and performed via a dual-luciferase reporter assay system (Promega).

RIP assays

RIP assays were performed using the Magna RIP RBP IP kit (Millipore) with the mouse anti-Ago2 antibody (Millipore) according to the manufacturer's instructions. Mouse anti-immunoglobulin G (IgG) antibody (Millipore) was used as a negative control.

Western blot and IP assay

For the western blot assay, total protein was extracted by protein lysis buffer, separated by SDS-PAGE gel, and transferred onto the polyvinylidene fluoride (PVDF) membrane (Millipore). After incubating with a primary antibody and corresponding secondary antibody, chemiluminescent reagent was used for detecting the signal of the membranes. For the IP assay, the primary antibodies were incubated with protein A/G magnetic beads (Sigma-Aldrich) at 4°C with gentle rotation for 3 h. Lysis was incubated with the beads for 2 h at 25°C, and the precipitated complex was subjected to western blot analysis. In this study, the following antibodies were used: GAPDH (AC002, ABclonal, Wuhan, China), STX3 (15556-1-AP; Proteintech, Wuhan, China), PTEN (9188; Cell Signaling Technology, Danvers, MA, USA), MRPS35 (16457; Proteintech), cleaved caspase-3 (9664; Cell Signaling Technology), ubiquitin (3936; Cell Signaling Technology), FLAG (AE005, ABclonal), goat anti-rabbit IgG horseradish peroxidase (HRP) conjugate (SA00001-1; Proteintech), and goat anti-mouse IgG HRP conjugate (SA00001-2; Proteintech).

In vivo ubiquitination assay

293T cells were transfected with combinations of plasmids (PLV-PTEN-FLAG, pCMV- HA-ubiquitin with or without PLV-STX3-Myc) for 48 h, and then cells were treated with or without 10 μg/mL MG132 (Sigma-Aldrich) for 12 h. Cells were lysed and the protein lysates were immunoprecipitated with anti-FLAG-A/G beads. Huh-7 and HCC-LM3 cells were treated with 10 μg/mL MG132 for 12 h and the protein lysates were immunoprecipitated with anti-PTEN-A/G beads. The precipitated complex was subjected to western blot analysis.
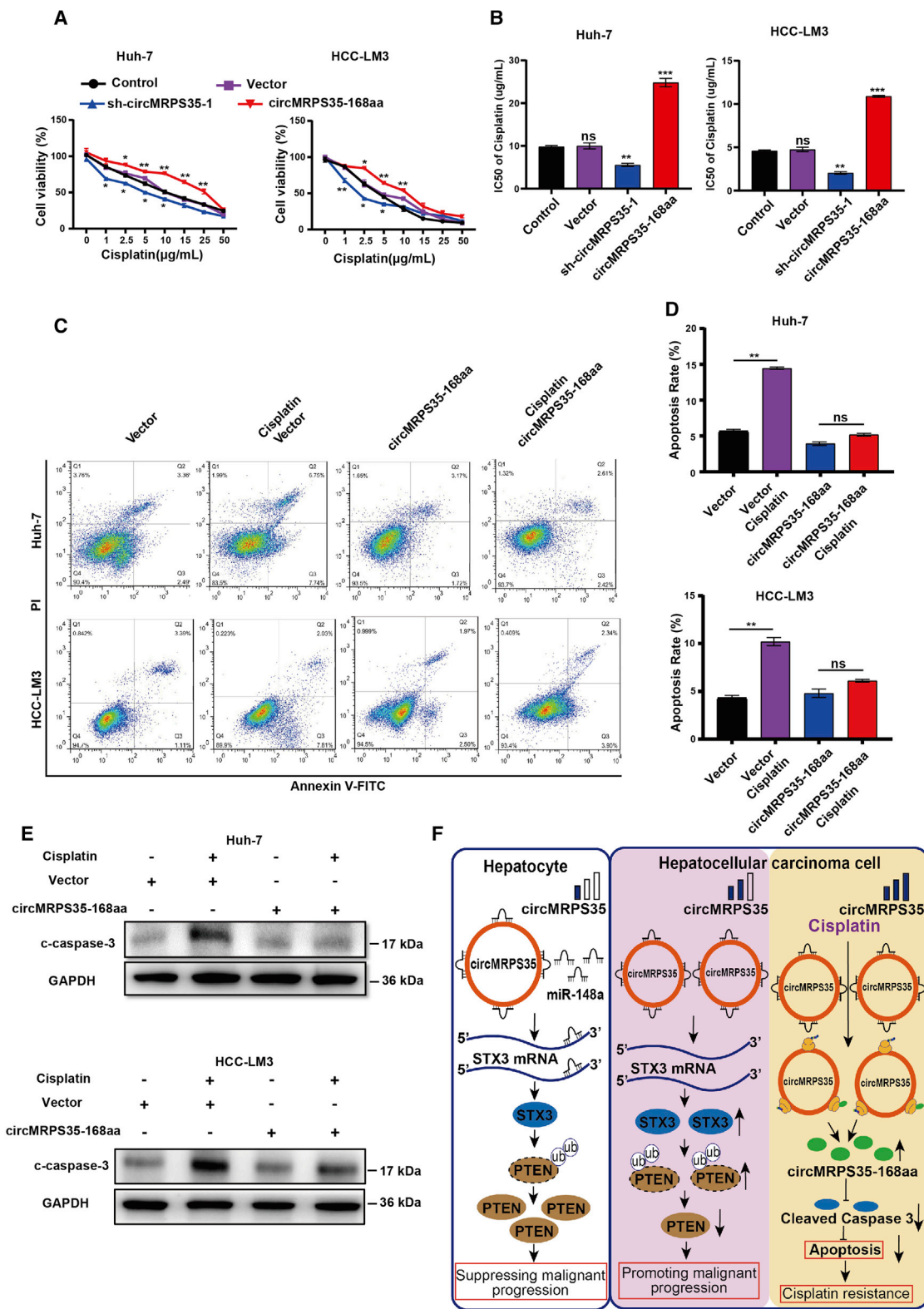
Cycloheximide (CHX) chase assay

Huh-7 and HCC-LM3 cells were treated with 10 μM CHX (Sigma-Aldrich) for (0, 1, 2, 4, and 8 h). Cell lysates were then subjected to western blot analysis.

In vivo xenograft assay

Four-week-old female BALB/c nude (nu/nu) mice were purchased from the Si Pei Fu (Beijing, China). Mice were housed under specific

---

Huh-7 cells (lower). The encephalomyocarditis virus (EMCV) IRES was used as a positive control. (D) Polysome fractionation and RT-PCR analysis of Huh-7 and HCC-LM3 cell lysate, with GAPDH as the positive control. (E and F) IP by FLAG antibody and SDS-PAGE separation of protein bands stained by Coomassie brilliant blue (CBB) and the band (red frame) (left) analyzed by LC-MS (right). (G) Western blot analysis of the expression of circMRPS35-168aa after treatment with five chemotherapy drugs in Huh-7 and HCC-LM3 cells, with GAPDH as the control. Error bars represent the means ± SEM of three independent experiments. *p < 0.05, **p < 0.01, ***p < 0.001.

A

Huh-7

HCC-LM3

● Control   ■ Vector
▲ sh-circMRPS35-1   ▼ circMRPS35-168aa

B

Huh-7

HCC-LM3

C

D

Huh-7

HCC-LM3

E

Huh-7

HCC-LM3

F

(legend on next page)

pathogen-free (SFP) conditions. Huh-7 and HCC-LM3 cells (2×10^6 cells) with different expression of circMRPS35 were subcutaneously injected in BALB/c nude mice. Tumor volumes were measured every 5 days and calculated using the following formula: volume (mm³) = (length $\times$ width²)/2. Tumor weights were determined 25 days after injection.

IHC assay

For immunostaining, sections were pretreated with hydrogen peroxide (3%) for 10 min to remove the endogenous peroxidase, followed by antigen retrieval in a microwave for 15 min in 10 mM citrate buffer (pH 6.0). Ki67 primary antibody (Ab15580; Abcam, Cambridge, MA, USA) was used at a dilution of 1:1,000 and incubated for 30 min at room temperature, followed by washing and incubation with the biotinylated secondary antibody for 30 min at room temperature and the stained with IHC staining kits (Boster, Beijing, China) according to the manufacturer's instructions. The slides were counterstained with hematoxylin and dehydrated in alcohol and xylene before mounting. The slides were imaged randomly with microscopy (Nikon).

Polysome fractionation assay

Huh-7 and HCC-LM3 cells were pre-treated with 200 μM CHX for 5 min at 37°C and washed with ice-cold PBS containing 200 μM CHX. Cells were then lysed with polysome lysis buffer for 30 min on ice. After centrifugation at 14,000 rpm for 10 min at 4°C, the supernatant was loaded onto 10-mL continuous 15%–50% sucrose gradient buffer containing 50 U/mL RNase inhibitor. The samples were centrifuged at 4°C for 3 h at $100,000 \times g$ by using an Avanti J-30XP (Beckman, Brea, CA, USA), and the fractions were collected using a Brandel fractionation system (Biocomp, Fredericton, NB, Canada), and an Isco UA-6 ultraviolet detector (Bio-Rad, Hercules, CA, USA) was used to produce polysome profiles for gradients. Extraction and transcription of total RNA from each fraction and RT-PCR were conducted as described above. GAPDH served as positive control.

LC-MS analysis

Proteins were separated via SDS-PAGE, and gel bands were manually excised and digested with sequencing-grade trypsin (Promega). The digested peptides were analyzed using a Q Exactive mass spectrometer (Invitrogen). Fragment spectra were analyzed using the National Center for Biotechnology Information nonredundant protein database with Mascot (Matrix Science, Boston, MA, USA).

Apoptosis analysis

Huh-7 and HCC-LM3 cells were resuspended and washed with PBS three times, and cells were stained with a cell apoptosis analysis kit (Beyotime) based on the manufacturer's instructions. Flow cytometry (BD Biosciences) was used to analyze the staining and the data were analyzed with FlowJo 7.6 software (Tree Star).

Chemotherapeutic drug treatment

Huh-7 and HCC-LM3 cells were reseeded in six-well plates (8×10^5 cells per well) overnight, and cells were then treated with 0.5 μg/mL DOX (Sigma-Aldrich), 50 μM etoposide (Sigma-Aldrich), 5 μg/mL cisplatin (Sigma-Aldrich), 0.2 μg/mL ACTD, and 10 μM sorafenib (Sigma-Aldrich), respectively. After a 24-h treatment, cells were collected for quantitative real-time PCR and western blot analysis.

IC$_{50}$ analysis

Huh-7 and HCC-LM3 cells were reseeded in 96-well plates (5×10^3 cells per well) overnight, and then cells were treated with DOX (0, 0.1, 0.2, 0.5, 1, 1.5, 3, and 5 μg/mL), etoposide (0, 5, 15, 25, 50, 100, 250, and 500 μM), cisplatin (0, 1, 2.5, 5, 10, 15, 25, and 50 μg/mL), and ACTD (0, 0.1, 0.15, 0.2, 0.5, 1, and 2.5 μg/mL), respectively, for 24 h. Cell viability was detected by CCK-8 kits (Beyotime) with absorbance of wavelength of 450 nm for each well. IC$_{50}$ was ensured based on the cell viability data.

Statistical analyses

All data are expressed as the mean ± SEM (standard error of the mean). Two-tailed unpaired or paired Student's t tests were applied to analyze the differences between two groups. Data conforming to normal distribution among multiple groups were analyzed by one-way or two-way analysis of variance (ANOVA). The values of *p < 0.05, **p < 0.01, and ***p < 0.001 are indicative of statistical significance, and ns is indicative of not significant. Statistical analyses were performed using GraphPad Prism 8.0. (GraphPad, La Jolla, CA, USA).

ETHICS STATEMENT

The use of human tissue specimens was approved by the Ethics Committee of the Chinese PLA General Hospital. All animal studies were approved by the Ethics Committee of the China Agricultural University. The study was performed in accordance with the Declaration of Helsinki.

Figure 7. circMRPS35-168aa resists cisplatin treatment in HCC cells

(A) Cell viability assay of different circMRPS35-168aa-expressed Huh-7 and HCC-LM3 cells with different concentrations of cisplatin treatment. (B) IC$_{50}$ analysis of different circMRPS35-168aa-expressed Huh-7 and HCC-LM3 cells with different concentrations of cisplatin treatment. (C and D) Fluorescence-activated cell sorting (FACS) analysis of apoptosis for different circMRPS35-168aa-expressed Huh-7 and HCC-LM3 cells with cisplatin treatment (left), and statistical analysis of apoptosis rate (right). (E) Western blot analysis of cleaved caspase-3 in different circMRPS35-168aa-expressed Huh-7 and HCC-LM3 cells with cisplatin treatment, with GAPDH as the control. (F) In this model, circMRPS35 elicited its oncogenic role in HCC via sponging miR-148a to regulate the expression of *STX3*, which modulated the ubiquitination and degradation of PTEN, and circMRPS35 was further upregulated in chemotherapeutic drug treatment that stimulated the coding of circMRPS35-168aa peptide. circMRPS35-168aa suppressed the cisplatin-induced apoptosis via inhibiting the cleavage of caspase-3, which led to cisplatin resistance. Error bars represent the means ± SEM of three independent experiments. *p < 0.05, **p < 0.01, ***p < 0.001.

SUPPLEMENTAL INFORMATION

Supplemental information can be found online at https://doi.org/10.1016/j.ymthe.2021.08.027.

AUTHOR CONTRIBUTIONS

X. Li signed the project, guided experiments, and analyzed data. P.L., R.S., and X. Li interpreted the data. P.L. conducted experiments. F.Y., M.L., and L.Y. collected and analyzed the clinical data and samples. R.S. and H.L. analyzed RNA-seq and TCGA data. Y.Z., S.M., X. Lu, and X.J. revised the manuscript. X. Li provided guidance for experiments. All authors approved the final content.

DECLARATION OF INTERESTS

The authors declare no competing interests.

REFERENCES

1. Bray, F., Ferlay, J., Soerjomataram, I., Siegel, R.L., Torre, L.A., and Jemal, A. (2018). Global cancer statistics 2018: GLOBOCAN estimates of incidence and mortality worldwide for 36 cancers in 185 countries. CA Cancer J. Clin. 68, 394–424.

2. Clark, T., Maximin, S., Meier, J., Pokharel, S., and Bhargava, P. (2015). Hepatocellular carcinoma: review of epidemiology, screening, imaging diagnosis, response assessment, and treatment. Curr. Probl. Diagn. Radiol. 44, 479–486.

3. Mazzoccoli, G., Miele, L., Oben, J., Grieco, A., and Vinciguerra, M. (2016). Biology, epidemiology, clinical aspects of hepatocellular carcinoma and the role of sorafenib. Curr. Drug Targets 17, 783–799.

4. Li, L., Chen, J., Chen, X., Tang, J., Guo, H., Wang, X., Qian, J., Luo, G., He, F., Lu, X., et al. (2016). Serum miRNAs as predictive and preventive biomarker for pre-clinical hepatocellular carcinoma. Cancer Lett. 373, 234–240.

5. Xiao, Y., Liu, G., Sun, Y., Gao, Y., Ouyang, X., Chang, C., Gong, L., and Yeh, S. (2020). Targeting the estrogen receptor alpha (ERα)-mediated circ-SMG1.72/miR-141-3p/Gelsolin signaling to better suppress the HCC cell invasion. Oncogene 39, 2493–2508.

6. Wei, L., Wang, X., Lv, L., Liu, J., Xing, H., Song, Y., Xie, M., Lei, T., Zhang, N., and Yang, M. (2019). The emerging role of microRNAs and long noncoding RNAs in drug resistance of hepatocellular carcinoma. Mol. Cancer 18, 147.

7. Kanthaje, S., Makol, A., and Chakraborti, A. (2018). Sorafenib response in hepatocellular carcinoma: MicroRNAs as tuning forks. Hepatol. Res. 48, 5–14.

8. Houseley, J.M., Garcia-Casado, Z., Pascual, M., Paricio, N., O'Dell, K.M.C., Monckton, D.G., and Artero, R.D. (2006). Noncanonical RNAs from transcripts of the Drosophila muscleblind gene. J. Hered. 97, 253–260.

9. Suzuki, H., and Tsukahara, T. (2014). A view of pre-mRNA splicing from RNase R resistant RNAs. Int. J. Mol. Sci. 15, 9331–9342.

10. Salzman, J., Chen, R.E., Olsen, M.N., Wang, P.L., and Brown, P.O. (2013). Cell-type specific features of circular RNA expression. PLoS Genet. 9, e1003777.

11. Han, D., Li, J., Wang, H., Su, X., Hou, J., Gu, Y., Qian, C., Lin, Y., Liu, X., Huang, M., et al. (2017). Circular RNA circMTO1 acts as the sponge of microRNA-9 to suppress hepatocellular carcinoma progression. Hepatology 66, 1151–1164.

12. Zhu, Y.J., Zheng, B., Luo, G.J., Ma, X.K., Lu, X.Y., Lin, X.M., Yang, S., Zhao, Q., Wu, T., Li, Z.X., et al. (2019). Circular RNAs negatively regulate cancer stem cells by physically binding FMRP against CCAR1 complex in hepatocellular carcinoma. Theranostics 9, 3526–3540.

13. Liang, W.C., Wong, C.W., Liang, P.P., Shi, M., Cao, Y., Rao, S.T., Tsui, S.K., Waye, M.M., Zhang, Q., Fu, W.M., and Zhang, J.F. (2019). Translation of the circular RNA circβ-catenin promotes liver cancer cell growth through activation of the Wnt pathway. Genome Biol. 20, 84.

14. Liu, Q., Cai, Y., Xiong, H., Deng, Y., and Dai, X. (2019). CCRDB: A cancer circRNAs-related database and its application in hepatocellular carcinoma-related circRNAs. Database (Oxford) 2019, baz063.

15. Ding, Y., Fang, A., Yan, J., Duan, J., Wang, N., Yi, Y., and Shen, C. (2019). Selective downregulation of distinct circRNAs in the tissues and plasma of patients with primary hepatic carcinoma. Oncol. Lett. 18, 5255–5268.

16. Zhen, N., Gu, S., Ma, J., Zhu, J., Yin, M., Xu, M., Wang, J., Huang, N., Cui, Z., Bian, Z., et al. (2019). circHMGCS1 promotes hepatoblastoma cell proliferation by regulating the IGF signaling pathway and glutaminolysis. Theranostics 9, 900–919.

17. Wang, B., Chen, H., Zhang, C., Yang, T., Zhao, Q., Yan, Y., Zhang, Y., and Xu, F. (2018). Effects of hsa_circRBM23 on hepatocellular carcinoma cell viability and migration as produced by regulating miR-138 expression. Cancer Biother. Radiopharm. 33, 194–202.

18. He, J., Huang, Z., He, M., Liao, J., Zhang, Q., Wang, S., Xie, L., Ouyang, L., Koeffler, H.P., Yin, D., and Liu, A. (2020). Circular RNA MAPK4 (circ-MAPK4) inhibits cell apoptosis via MAPK signaling pathway by sponging miR-125a-3p in gliomas. Mol. Cancer 19, 17.

19. Ha, M., and Kim, V.N. (2014). Regulation of microRNA biogenesis. Nat. Rev. Mol. Cell Biol. 15, 509–524.

20. Nan, H., Han, L., Ma, J., Yang, C., Su, R., and He, J. (2018). STX3 represses the stability of the tumor suppressor PTEN to activate the PI3K-Akt-mTOR signaling and promotes the growth of breast cancer cells. Biochim. Biophys. Acta Mol. Basis Dis. 1864 (5 Pt A), 1684–1692.

21. Zhao, J., Lee, E.E., Kim, J., Yang, R., Chamseddin, B., Ni, C., Gusho, E., Xie, Y., Chiang, C.M., Buszczak, M., et al. (2019). Transforming activity of an oncoprotein-encoding circular RNA from human papillomavirus. Nat. Commun. 10, 2300.

22. Yang, Y., Fan, X., Mao, M., Song, X., Wu, P., Zhang, Y., Jin, Y., Yang, Y., Chen, L.L., Wang, Y., et al. (2017). Extensive translation of circular RNAs driven by N^6-methyladenosine. Cell Res. 27, 626–641.

23. Cheng, Y., Sun, H., Wang, H., Jiang, W., Tang, W., Lu, C., Zhang, W., Chen, Z., and Lv, C. (2019). Star circular RNAs in human cancer: Progress and perspectives. OncoTargets Ther. 12, 8249–8261.

24. Kristensen, L.S., Andersen, M.S., Stagsted, L.V.W., Ebbesen, K.K., Hansen, T.B., and Kjems, J. (2019). The biogenesis, biology and characterization of circular RNAs. Nat. Rev. Genet. 20, 675–691.

25. Meng, X., Li, X., Zhang, P., Wang, J., Zhou, Y., and Chen, M. (2017). Circular RNA: An emerging key player in RNA world. Brief. Bioinform. 18, 547–557.

26. Gailhouste, L., Gomez-Santos, L., Hagiwara, K., Hatada, I., Kitagawa, N., Kawaharada, K., Thirion, M., Kosaka, N., Takahashi, R.U., Shibata, T., et al. (2013). miR-148a plays a pivotal role in the liver by promoting the hepatospecific phenotype and suppressing the invasiveness of transformed cells. Hepatology 58, 1153–1165.

27. Xu, X., Fan, Z., Kang, L., Han, J., Jiang, C., Zheng, X., Zhu, Z., Jiao, H., Lin, J., Jiang, K., et al. (2013). Hepatitis B virus X protein represses miRNA-148a to enhance tumorigenesis. J. Clin. Invest. 123, 630–645.

28. Li, L., Liu, Y., Guo, Y., Liu, B., Zhao, Y., Li, P., Song, F., Zheng, H., Yu, J., Song, T., et al. (2015). Regulatory miR-148a-ACVR1/BMP circuit defines a cancer stem cell-like aggressive subtype of hepatocellular carcinoma. Hepatology 61, 574–584.

29. Wang, F., Ying, H., He, B., Pan, Y., Sun, H., and Wang, S. (2016). Circulating miR-148/152 family as potential biomarkers in hepatocellular carcinoma. Tumour Biol. 37, 4945–4953.

30. Han, J., Li, J., Qian, Y., Liu, W., Liang, J., Huang, Z., Wang, S., and Zhao, C. (2019). Identification of plasma miR-148a as a noninvasive biomarker for hepatocellular carcinoma. Clin. Res. Hepatol. Gastroenterol. 43, 585–593.

31. Delgrossi, M.H., Breuza, L., Mirre, C., Chavrier, P., and Bivic, A.L. (1997). Human syntaxin 3 is localized apically in human intestinal cells. J. Cell Sci. *110*, 2207–2214.

32. Zhao, Z.Z., Duffy, D.L., Thomas, S.A., Martin, N.G., Hayward, N.K., and Montgomery, G.W. (2009). Polymorphisms in the syntaxin 17 gene are not associated with human cutaneous malignant melanoma. Melanoma Res. *19*, 80–86.

33. Frank, S.P., Thon, K.P., Bischoff, S.C., and Lorentz, A. (2011). SNAP-23 and syntaxin-3 are required for chemokine release by mature human mast cells. Mol. Immunol. *49*, 353–358.

34. Terazawa, T., Kondo, S., Hosoi, H., Morizane, C., Shimizu, S., Mitsunaga, S., Ikeda, M., Ueno, H., and Okusaka, T. (2014). Transarterial infusion chemotherapy with cisplatin plus S-1 for hepatocellular carcinoma treatment: A phase I trial. BMC Cancer *14*, 301.

35. Ding, K., Fan, L., Chen, S., Wang, Y., Yu, H., Sun, Y., Yu, J., Wang, L., Liu, X., and Liu, Y. (2015). Overexpression of osteopontin promotes resistance to cisplatin treatment in HCC. Oncol. Rep. *34*, 3297–3303.

36. Ding, B., Lou, W., Xu, L., and Fan, W. (2018). Non-coding RNA in drug resistance of hepatocellular carcinoma. Biosci. Rep. *38*, BSR20180915.

37. Guan, Y., Zhang, Y., Hao, L., and Nie, Z. (2020). circRNA_102272 promotes cisplatin-resistance in hepatocellular carcinoma by decreasing miR-326 targeting of RUNX2. Cancer Manag. Res. *12*, 12527–12534.

38. Kalkavan, H., and Green, D.R. (2018). MOMP, cell suicide as a BCL-2 family business. Cell Death Differ. *25*, 46–55.

39. Jin, Z., and El-Deiry, W.S. (2005). Overview of cell death signaling pathways. Cancer Biol. Ther. *4*, 139–163.

40. Jie, M., Wu, Y., Gao, M., Li, X., Liu, C., Ouyang, Q., Tang, Q., Shan, C., Lv, Y., Zhang, K., et al. (2020). circMRPS35 suppresses gastric cancer progression via recruiting KAT7 to govern histone modification. Mol. Cancer *19*, 56.

41. Conn, S.J., Pillman, K.A., Toubia, J., Conn, V.M., Salmanidis, M., Phillips, C.A., Roslan, S., Schreiber, A.W., Gregory, P.A., and Goodall, G.J. (2015). The RNA binding protein quaking regulates formation of circRNAs. Cell *160*, 1125–1134.

42. Errichelli, L., Dini Modigliani, S., Laneve, P., Colantoni, A., Legnini, I., Capauto, D., Rosa, A., De Santis, R., Scarfò, R., Peruzzi, G., et al. (2017). FUS affects circular RNA expression in murine embryonic stem cell-derived motor neurons. Nat. Commun. *8*, 14741.

43. Li, Y., Chen, B., Zhao, J., Li, Q., Chen, S., Guo, T., Li, Y., Lai, H., Chen, Z., Meng, Z., et al. (2021). HNRNPL circularizes ARHGAP35 to produce an oncogenic protein. Adv. Sci. (Weinh.) *8*, 2001701.

44. Zhang, J., Chen, S., Yang, J., and Zhao, F. (2020). Accurate quantification of circular RNAs identifies extensive circular isoform switching events. Nat. Commun. *11*, 90.